Pergamon

Int. J. Heat Mass Transfer. Vol. 41, No. 12, pp. 1633–1643, 1998

Printed in Great Britain
0017–9310/98 $19.00+0.00

PII: S0017–9310(97)00304–9

Numerical prediction of turbulent mixed convection in a concentric horizontal rotating annulus with low-*Re* two-equation models

MING-I CHAR† and YUAN-HSIUNG HSU

Department of Applied Mathematics, National Chung Hsing University, Taichung, Taiwan 402, R.O.C.

(*Received* 31 *May* 1996 *and in final form* 30 *September* 1997)

Abstract—Numerical computations are conducted for turbulent mixed convection of air in a horizontal concentric annulus between a cooled outer cylinder and a heated, rotating, inner cylinder. Time-averaged equations of turbulent fluid motion and heat transfer are solved using the Launder–Sharma low-*Re* eddy-viscosity two-equation model coupled with the Yap correction and the Kato–Launder modification. Numerical results are obtained for the Rayleigh number, *Ra*, ranging from 10^7 to 10^{10}, the Reynolds number, *Re*, from 0 to 10^5 and the radius ratio, *RR*, from 2.6 to 10 for a constant Prandtl number of 0.7. The effects of these parameters on the flow and heat transfer characteristics are discussed in detail. Predictions are also compared with published studies of other investigators. A good agreement with the results from the published experimental data and other computations is found. A comprehensively comparative analysis shows that the Kato–Launder modification is an essential ingredient, which can effectively reduce the unrealistic turbulence energy at impingement regions. Therefore, the modification can return more satisfactory prediction for the considered cases. Results show that the mean Nusselt number, $\overline{Nu}$, increases with an increase in *Ra*, but decreases with an increase in *Re* or *RR*. When $Ra > 10^9$, a crucial phenomena, the peak value of local Nusselt number occurring in the vicinity of thermal plume region, is first discovered and discussed. For the centrifugal configurations, it is found that rotation has caused significant reduction in the mean heat transfer and it generally increases the strength of the secondary flows.

1. INTRODUCTION

The problem of the buoyancy-driven turbulent flow in a concentric rotating system has recently attracted considerable attention because of its numerous applications. Such applications are encountered in seeking improvements for crystallographic perfection in industrial process [1, 2], food processes [3], heat removal from nuclear reactor fuel rods, and underground electric transmission cable using pressurized gas. Although the influence of rotation, especially for a higher angular velocity, on the turbulent convective flow is important, very little work has been reported in the literature. In the turbulent mixed convection problem, rotation affects not only on the mean flow through Coriolis force but also, in a more subtle manner, directly on the fluctuating motion itself.

During the last few years, many numerical investigations pertain to the turbulent flow in the stationary annulus. Also, relatively little amount of experimental work has been made to investigate buoyancy-induced annular flow in the turbulent regime. Kuehn and Goldstein [4] measured the heat transfer coefficients in air and water in concentric and eccentric horizontal annuli. Recently, Bishop [5] reported an experimental investigation of turbulent natural convection of helium between horizontal isothermal concentric cylinders at cryogenic temperature. He measured overall heat transfer rates and time-averaged temperature profiles for the Prandtl number $Pr = 0.688$, radius ratio $RR = 3.36$, with the Rayleigh numbers, based on gap thickness, ranging from 6×10^6 to 2×10^9, and with the expansion numbers from 0.25–1.0. Later, Mcleod and Bishop [6] used the same experimental apparatus of Bishop [5] to obtain the temperature fluctuations for helium at $RR = 4.85$. It was found that the heat transfer rates depend on the magnitude of the expansion number as well as on the Rayleigh number.

Because of the viscous shearing effects at the end walls, a three-dimensional analysis of the turbulent natural convection flow, in general, is needed when the annulus has a finite length. More recently, turbulent transport in a horizontal cylindrical annulus has been modeled by Desai and Vafai [7], employing the k–ε turbulence model. Their results revealed that, if the annulus is sufficiently long (when the annulus length is 7.5 times larger than the gap between inner and outer cylinders), there exists a core region over a substantial length of the cavity, which could be approximated by a two-dimensional approach. Farouk and Guceri [8] used the k–ε turbulence model proposed first by Launder and Spalding [9] to simulate the

† Author to whom correspondence should be addressed.

NOMENCLATURE

g_i	gravitational acceleration vector, $(0, -g)$
k	turbulent kinetic energy
L	gap width, $R_o - R_i$
n	normal vector on the wall
Nu, $\overline{Nu}$	local and mean Nusselt number
P	pressure
P_k	turbulent production
Pr	molecular Prandtl number
r	radial coordinate
R_i, R_o	radius of the inner and outer cylinders
RR	radius ratio, R_o/R_i
Ra	Rayleigh number, $g\beta L^3(\Theta_i - \Theta_o)/v\alpha$
Re	Reynolds number of the inner cylinder, $R_i\omega L/v$
$\overline{u_i u_j}$	Reynolds stress tensor
$\overline{u_i\theta}$	kinematic turbulent heat flux
U, V	mean-velocity components at X- and Y-directions
U_i	mean velocity in the X_i direction
y	the distance from the wall
y^+	dimensionless value of y, $y(\tau_w\rho)^{1/2}/\mu$.

Greek symbols

α	thermal diffusivity
β	coefficient of volumetric expansion
ε	turbulence energy dissipation rate
$\tilde{\varepsilon}$	isotropic part of ε associated with spectral transfer, $\varepsilon - 2v[k_j^{1/2}]^2$
θ	temperature fluctuation
Θ	temperature
Θ_i, Θ_o	temperature of inner and outer cylinders
μ, μ_t	dynamic and turbulent viscosity
μ_t^*	dimensionless turbulent viscosity, μ_t/μ
v, v_t	kinematic and eddy viscosity
ρ	density
σ_θ	turbulent Prandtl number for θ transport
τ_w	shear stress on the wall
ϕ	azimuthal angle measured from the positive Y axis
Ψ	stream function
ω	rotating speed of the inner cylinder.

steady-state, two-dimensional natural convection in the annulus. The results were obtained for Rayleigh number range of 10^6–10^7 at a fixed radius ratio of 2.6. Still, the natural convection flow in a cavity with different turbulent models was studied by Henkes *et al.* [10]. As compared with the experimental data, they found that the low-Reynolds number k–ε model gave better predictions than the standard k–ε model with wall functions.

In this study, simulations of turbulent mixed convection in the concentric horizontal rotating cylinders have been investigated. Turbulence model adopted here is the low-Reynolds number k–ε model proposed by Launder and Sharma [11] in conjunction with the Yap correction [12] and the Kato–Launder modification [13]. It is known that in boundary layers approaching separation the k–ε model returns near-wall length scales which are too large [12, 14]. The turbulence energy generated far from the wall is diffused toward the surface. To overcome this weakness, an extra source term in the ε equation is added, originally devised by Yap [12] to prevent excessive near-wall length scales developing in separated flows. In addition, a well-known defect of the Launder–Sharma model is that it always overpredicts turbulence energy at the impingement region due to large generation of the turbulent kinetic energy. To remedy this deficiency, the Kato–Launder modification [13] is implemented to depress the turbulence energy in the vicinity of impingement region. The rationale of these two modifications will be further discussed in the next section. The predictions are compared to numerical and experimental results available in the literature. The effects of the Rayleigh and Reynolds numbers and the radius ratio on the mean Nusselt number are investigated in detail.

Recently, Kenjereš and Hanjalić [15] have performed a numerical simulation for turbulent natural convection within annuli using a k–ε–$\overline{\theta^2}$ model. The authors demonstrated that the model can achieve fairly good predictions for mean temperature and the local Nusselt number. However, this model involves a further differential equation for $\overline{\theta^2}$ which introduces more coupling among variables and inevitably increases the CPU demands. Similar, not necessarily as good, improvement can also be obtained by the present modelling approach which is much simpler and requires no further increase in CPU time.

2. MATHEMATICAL MODELLING

The present work focuses on the problem of turbulent mixed convection flows enclosed in the annuli, consisting of two concentric horizontal cylinders with the heated, rotating inner one. A schematic diagram of the physical model and coordinate system is shown in Fig. 1. In the analysis, we now assume that the flow is steady and the thermophysical properties of the fluid are taken to be constant, except for the density in the buoyancy term in the momentum equations. If the annulus length is sufficiently large compared to gap-width (the annulus length to gap-width ratio of

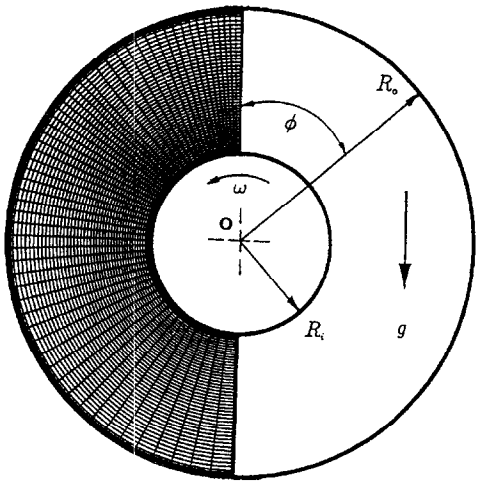

Fig. 1. The physical model and coordinate system.

at least 7.5), the viscous shearing effects at the end walls can be neglected [7]. Therefore, the Boussinesq approximation and the two-dimensional model are applicable. To this end, equations describing the mean flow and temperature in the annulus can be given as:

$$U_{j,j} = 0 \tag{1}$$

$$U_j U_{i,j} = -\frac{1}{\rho} P_{,i} - g_i \beta \Theta + [\nu(U_{i,j} + U_{j,i}) - \overline{u_i u_j}]_{,j}, \tag{2}$$

$$U_j \Theta_{,j} = \left[\left(\alpha + \frac{\nu_t}{\sigma_\theta}\right)\Theta_{,j}\right]_{,j}. \tag{3}$$

The relationship between Reynolds-stresses and mean strains are:

$$\overline{u_i u_j} = \tfrac{2}{3}\delta_{ij} k - \nu_t [U_{i,j} + U_{j,i}]. \tag{4}$$

Within the low-Re k–ε eddy-viscosity framework, the turbulent viscosity ν_t arises as:

$$\nu_t = C_\mu f_\mu \frac{k^2}{\tilde{\varepsilon}}, \tag{5}$$

where the turbulence energy k and $\tilde{\varepsilon}$ (the isotropy part of the turbulence energy dissipation rate) are determined from the following transport equations:

$$U_j k_{,j} = [(\nu + \nu_t) k_{,j}]_{,j} + P_k - g_i \beta \overline{u_i \theta} - \varepsilon \tag{6}$$

$$U_j \tilde{\varepsilon}_{,j} = \left[\left(\nu + \frac{\nu_t}{1.3}\right)\tilde{\varepsilon}_{,j}\right]_{,j} + \frac{\tilde{\varepsilon}}{k}[C_{\varepsilon 1}(P_k - g_i \beta \overline{u_i \theta}) - C_{\varepsilon 2}\tilde{\varepsilon}]$$

$$+ 2\nu\nu_t [U_{i,jk}]^2 + 0.83\left[\frac{k^{3/2}}{\tilde{\varepsilon} C_{\varepsilon 3} y} - 1\right]\left[\frac{k^{3/2}}{\tilde{\varepsilon} C_{\varepsilon 3} y}\right]^2 \frac{\tilde{\varepsilon}^2}{k}. \tag{7}$$

Turbulent heat flux vector is approximated by:

$$\overline{u_i \theta} = \frac{\nu_t}{\sigma_\theta} \Theta_{,i} \tag{8}$$

where $\sigma_\theta = 0.9$. In these equations, ε, the total dissipation rate of k, equals $\tilde{\varepsilon} + 2\nu[k_{,j}^{1/2}]^2$ while P_k denotes the generation rate of turbulence energy. Here, only the Launder–Sharma model [11] is investigated, both in its original form and in conjunction with Kato–Launder modification [13] pertaining to the production term P_k, namely:

$$P_k = C_\mu f_\mu \tilde{\varepsilon} \tilde{S}^2 \quad \text{(Launder and Sharma [11])}$$

$$P_k = C_\mu f_\mu \tilde{\varepsilon} \tilde{S} \tilde{\Omega} \quad \text{(Kato and Launder [13]).} \tag{9}$$

The various coefficients are prescribed as follows:

$$C_\mu = 0.09, \; f_\mu = \exp\left[-\frac{3.4}{(1 + R_t/50)^2}\right], \; R_t = \frac{k^2}{\nu\tilde{\varepsilon}},$$

$$C_{\varepsilon 1} = 1.44, \; C_{\varepsilon 2} = 1.92[1 - 0.3\exp(-R_t^2)], \; C_{\varepsilon 3} = 2.4$$

$$\tilde{S} = \frac{k}{\tilde{\varepsilon}}\sqrt{0.5(U_{i,j} + U_{j,i})^2}, \quad \tilde{\Omega} = \frac{k}{\tilde{\varepsilon}}\sqrt{0.5(U_{i,j} - U_{j,i})^2}. \tag{10}$$

The boundary conditions for this problem, with heated inner cylinder rotating at an angular velocity ω, can be given as: no-slip conditions of the velocity at the boundary, uniform but different temperatures of the inner and outer cylinders, and vanishing of the pressure gradient on the boundary. Thus, the boundary conditions are:

$$r = R_i: U = -R_i\omega\cos\phi, \quad V = R_i\omega\sin\phi,$$

$$\frac{\partial P}{\partial n} = 0, \quad \Theta = \Theta_i, \quad k = 0, \quad \tilde{\varepsilon} = 0$$

$$r = R_o: U = 0, \quad V = 0, \quad \frac{\partial P}{\partial n} = 0, \quad \Theta = \Theta_o$$

$$k = 0, \quad \tilde{\varepsilon} = 0. \tag{11}$$

The governing parameters of Ra, Re and RR, are given as follows:

$$Ra = g\beta L^3(\Theta_i - \Theta_o)/\nu\alpha,$$

$$Re = R_i\omega L/\nu, \quad RR = R_o/R_i \tag{12}$$

where Θ_i and Θ_o are temperature at inner and outer cylinders, respectively. The dimensionless parameters are

$$k^* = L^2 k/\nu^2, \quad \Psi^* = \Psi/\nu, \quad \mu_t^* = \mu_t/\mu. \tag{13}$$

As mentioned, there are two modifications to the original Launder–Sharma model in the present computation. First, the last term in the $\tilde{\varepsilon}$ equation is the near-wall length-scale correction (the Yap correction [12]) mentioned in the introduction section, where y is the distance from the wall. This term acts to decrease turbulence length scale when it is larger than the local equilibrium value $2.4y$. The second and more important modification is made to the turbulence production term P_k. It is known that Launder–Sharma model and other similar models always overpredicts turbulence energy at impingement region due to the formula of P_k. Thus, this leads to the overestimation of turbulence viscosity, μ_t. When μ_t is overestimated,

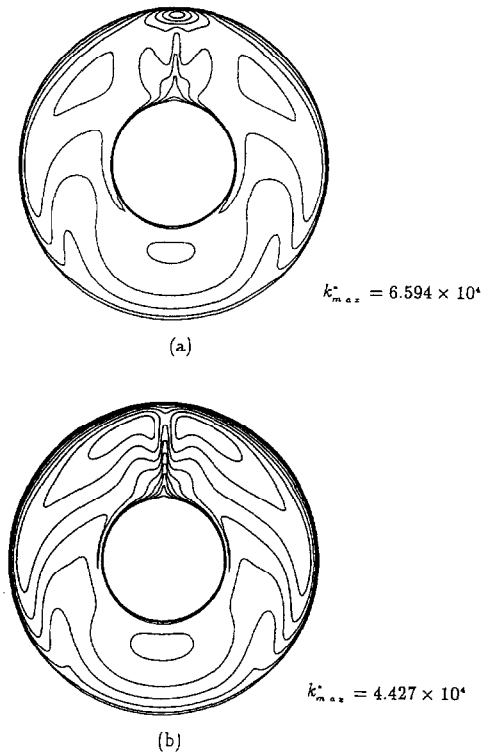

Fig. 2. Time-averaged turbulent K.E. at $Ra = 2.51 \times 10^6$, $Re = 0$, $RR = 2.6$ and $Pr = 0.7$: (a) Launder–Sharma model; and (b) Kato–Launder modification.

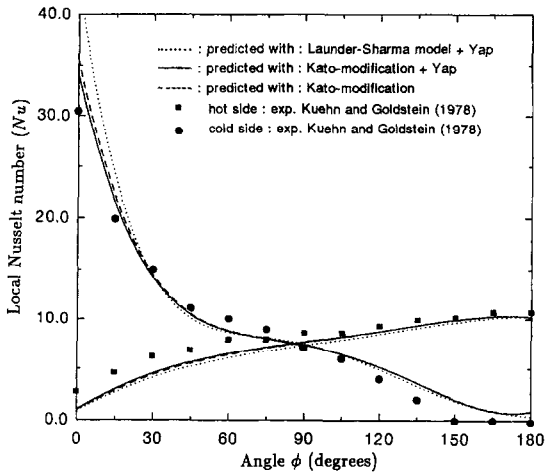

Fig. 3. Local Nusselt number distributions for a test case with $Ra = 2.51 \times 10^6$, $Re = 0$, $RR = 2.6$ and $Pr = 0.731$ in a concentric annulus.

heat transfer in the region will be unrealistically enhanced through equation (3). The defect can be easily resolved by the introduction of Kato–Launder modification [13]. This modification simply replaces $\tilde{S}^2$ in P_k by $\tilde{S}\tilde{\Omega}$. The idea is that $\tilde{\Omega}$ is approaching zero at the impingement region, leading to a significant reduction of P_k at the region, hence, μ_t is effectively decreased and so is the heat transfer.

The effects of Kato–Launder modification can be demonstrated by Fig. 2, the contour of turbulence energy upon the impingement region where a thermal plume arising from inner cylinder hits the wall of the outer cylinder. As seen, the Launder–Sharma model predicts very large turbulence energy around impingement point. The Kato–Launder modification, on the other hand, greatly reduces turbulence energy and then improves heat transfer prediction. The advantage of this modification is easily demonstrated by the comparison of the local Nusselt number with experimental data shown in Fig. 3. In this figure, the coupled Kato–Launder and Yap modifications give a much closer prediction than that of the Launder–Sharma model. Thus, the modifications can effectively reduce the unrealistic turbulence energy at impingement regions. In order to identify the primary modification which contributes to the above improvement, results obtained by applying only Kato–Launder modification are also in Fig. 3. One can see that the results are close to those obtained with both modifications. Therefore, the Kato–Launder modification is of primary importance to the reduction of turbulence energy upon impingement. In the following, computations are performed with the use of both Yap correction and Kato–Launder modification.

3. NUMERICAL PROCEDURE

Calculations have been performed with the general non-orthogonal, fully collocated finite-volume approach STREAM [16]. Advective volume-face fluxes are approximated using van Leer's MUSCL scheme [17]. The velocity components, pressure and temperature are stored together at cell-centered nodes. At all speeds, mass continuity is enforced by solving the pressure-correction equation. The usual sequence of operations may be performed precisely in the same manner as detailed by Patankar SIMPLE [18] procedure for the staggered arrangement.

3.1. *Calculation of* Nu *and* $\overline{\text{Nu}}$

The local Nusselt numbers for the inner and outer cylinder walls are defined, respectively, as:

$$Nu_i = \frac{-R_i}{\Theta_i - \Theta_o} \ln\left(\frac{R_o}{R_i}\right) \left.\frac{\partial \Theta}{\partial r}\right|_{r=R_i},$$

$$Nu_o = \frac{-R_o}{\Theta_i - \Theta_o} \ln\left(\frac{R_o}{R_i}\right) \left.\frac{\partial \Theta}{\partial r}\right|_{r=R_o}. \quad (14)$$

The mean Nusselt number is determined from:

$$\overline{Nu_i} = \frac{1}{2\pi}\int_0^{2\pi} Nu_i \, d\phi, \quad \overline{Nu_o} = \frac{1}{2\pi}\int_0^{2\pi} Nu_o \, d\phi,$$

$$\overline{Nu} = \frac{1}{2}(\overline{Nu_i} + \overline{Nu_o}). \quad (15)$$

4. RESULTS AND DISCUSSION

A wide range of parameters ($10^7 \leqslant Ra \leqslant 10^{10}$, $0 \leqslant Re \leqslant 10^5$, $2.6 \leqslant RR \leqslant 10$) was considered in the present study. Some values were chosen to facilitate comparisons with published experimental and numerical data. The majority of the numerical results presented here are through streamlines and isotherms. The local and mean heat transfer results were then given by plots showing the Nusselt number variation with the angular position along the inner and outer cylinders for the discussion of the interaction between fluid flow and heat transfer.

To examine the grid independency, computations for velocity and Nusselt number in a concentric stationary annulus with $RR = 2.6$, $Ra = 10^9$ and $Pr = 0.7$ are carried out using three different meshes, 61×41, 121×81 and 181×121. The local Nusselt number variation over both cylinders as a function of the angular position for different mesh sizes is shown in Fig. 4. In fact, refinement from 121–181 nodes only makes 1% changes in maximum velocity and the mean Nusselt number, hence further refinements are thought to bring negligible change. This indicates that grid independent solutions can be obtained by 121×81 mesh. However, to ensure y^+ of the first node is always less than unity, the nonuniform 121×181 mesh is used for computing lower Ra number cases, and the 181×121 mesh, for higher Ra number cases.

Based on the finer near-wall mesh, one can find an interesting phenomena which the local Nusselt number distribution decreases firstly then increases later in the vicinity of zero-degree region. In this higher Ra regime, the combined action of inertial and wall-viscous force initiates a reverse eddy flow at the plume root region. This phenomena is exemplified in Fig. 5. It can be seen that as long as the reverse eddy flow occurs, more viscous dissipation makes the flow velocity lower, hence, which leads to the decrease of heat transfer. These are the reasons for the peak phenomena occurring near the zero-degree region in Fig. 4. If a coarse mesh is adopted in the higher Ra cases, it can not provide a theoretical view of near-wall viscous effect in this region. Therefore, a finer near-wall mesh is thus necessary to predict accurately the wall-viscosity effect and the heat transfer characteristic.

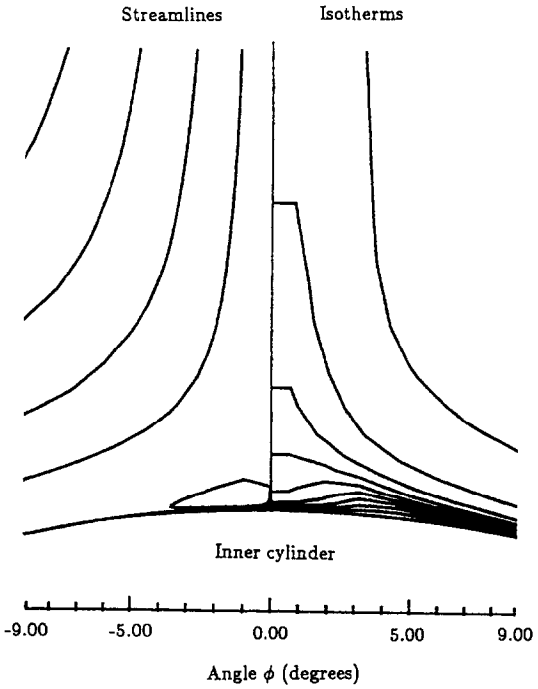

Fig. 5. Streamlines and isotherms in the vicinity of thermal plume region—$Ra = 10^9$, $Re = 0$, $RR = 2.6$ and $Pr = 0.7$.

As far as the authors' knowledge, no experimental data could be found in the literature for the turbulent mixed convection flow with the geometry and boundary conditions studied here. Hence, the validation of

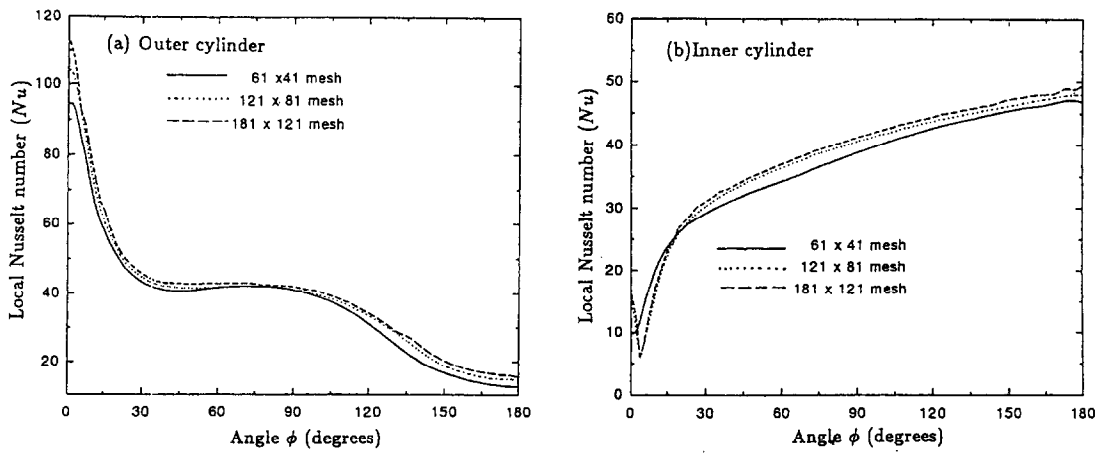

Fig. 4. Grid-size independence of local Nusselt number values—$Ra = 10^9$, $Re = 0$, $RR = 2.6$ and $Pr = 0.7$: (a) outer cylinder; and (b) inner cylinder.

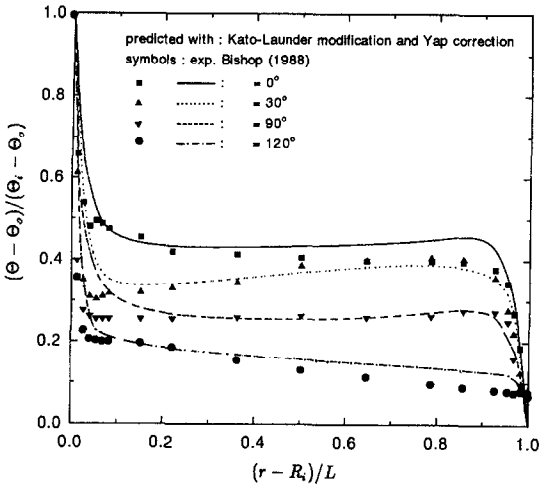

Fig. 6. Mean-temperature profiles for a test case with $Ra = 1.15 \times 10^9$, $Re = 0$, $RR = 3.36$ and $Pr = 0.688$ in a concentric annulus.

the turbulent model can only be performed in natural convection stationary annulus cases where experimental data are available. In Fig. 3, the local Nusselt number distribution at $Ra = 2.51 \times 10^6$, $Pr = 0.7$ and $RR = 2.6$ for inner and outer cylinders shows that the present results are in good agreement with the experimental data of Kuehn and Goldstein [4]. Another comparison with the experimental data in a horizontal annulus at cryogenic temperatures performed by Bishop [5] is given in Fig. 6. In this test case, the outer and inner radius ratio RR, Rayleigh number Ra and expansion number $\beta\Delta T$ are 3.36, 1.15×10^9 and 0.5, respectively. The dimensionless mean-temperature profiles at different cross sections show good agreement with the experimental data.

4.1. *Effect of Reynolds number*

Figure 7 illustrates the influence of forced convection due to the rotating inner cylinder on the mixed convection flow structure and temperature field at various Reynolds number with fixed $RR = 2.6$ and $Pr = 0.7$ at $Ra = 10^8$. As seen from these contours, when Re increases, the basic structures of the flow field consist of: the predominant growth of the right-hand cell; the increase of the intensity of stream-function appearing around the inner cylinder; the rise of the thermal plume tending to the descending side; the decrease of the thickness of the thermal boundary layer along the inner cylinder; and the more monotonic and asymmetric contours in the annulus gap. When Re increases up to 10^5, it can be seen that separation flow is diminished and the concentric circulation appears, resembling the uniform flow observed in isothermal flow configuration. This is a clear indication of a centrifugally dominated flow structure.

The effects of rotation on the local Nusselt number are illustrated in Fig. 8. An overview of these figures shows that the increase in Re causes the location of maximum local heat flux on the outer cylinder moving to the descending side, and the peak value of the local Nusselt number is reduced. The point of minimum local heat flux on the inner cylinder, which corresponds to the location of the root of the thermal plume, also moves in the same way while the peak value increases. At constant Ra, Table 1 shows that the mean Nusselt number $\overline{Nu}$ decreases with increasing Re because the centrifugal effects reduce the total heat transfer. With stronger rotation, the centrifugal effects become more important in the vicinity of the inner cylinder, which increases the isotherm space and a corresponding reduction in $\overline{Nu}$ around the inner cylinder.

4.2. *Effect of Rayleigh number*

Figure 9 depicts the streamlines and isotherms for various Rayleigh number with fixed $Re = 10^4$, $RR = 2.6$ and $Pr = 0.7$. As seen from these figures, stronger buoyant effect results in more symmetric pattern of these contours. When Ra increases, the intensities of the recirculation, turbulent energy and turbulent viscosity are increased. The isotherms become closer along surfaces of inner and outer cylinders as Ra increases, and large temperature gradients come up accordingly which lead to higher local heat flux around inner and outer cylinders. The local Nusselt number, Nu, distributions are illustrated in Fig. 10. When Ra increases, the buoyancy-driven flow becomes more predominant, the maximum local heat flux on the outer cylinder and the minimum local heat flux on the inner cylinder are increased and moved

Table 1. Mean Nusselt number $\overline{Nu}$ for various cases studied

Parameter Ra =	10^7		10^8	10^9				10^{10}
RR =	2.6	5.0	2.6	2.6	3.5	5.0	10.0	2.6
$Re = 0$	10.286	9.953	21.823	42.084	40.932	38.179	36.231	86.432
$Re = 10^2$	10.129	9.578	20.826	41.937				
$Re = 10^3$	10.006	9.162	20.512	41.672				
$Re = 10^4$	8.826	7.583	19.340	41.328	39.541	35.621	30.074	85.478
$Re = 10^5$	6.091	5.211	15.832	40.803				

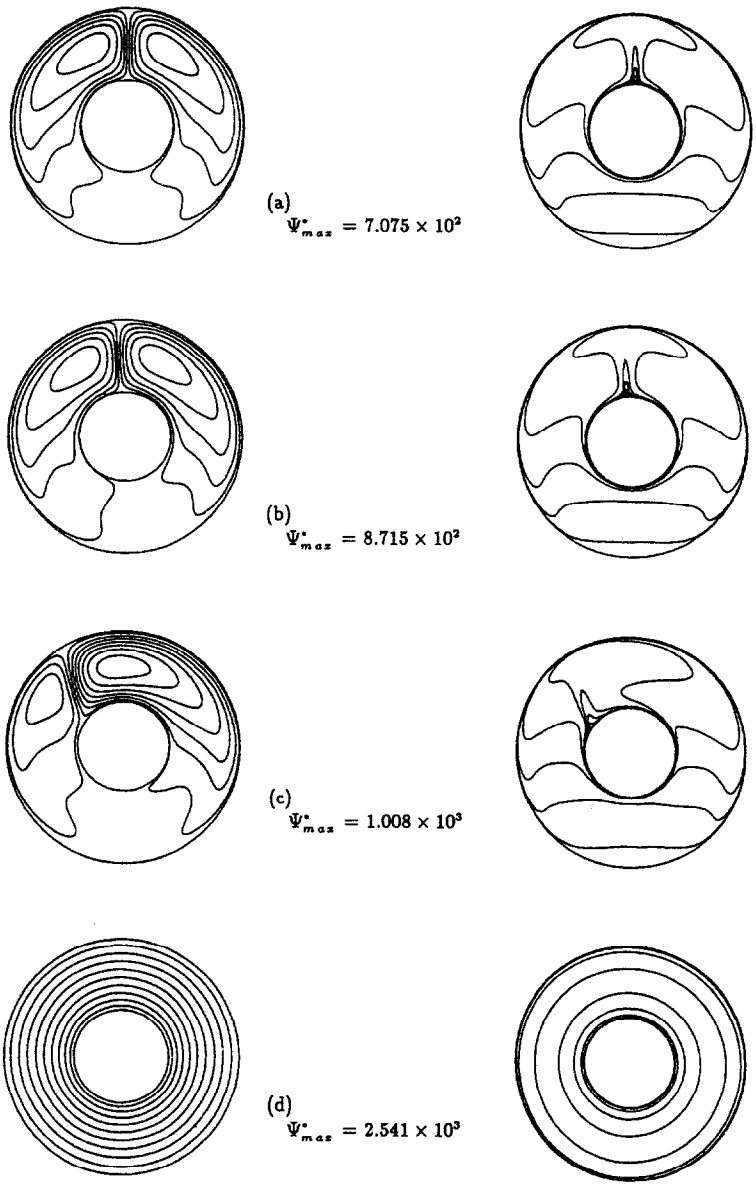

Fig. 7. Streamlines and isotherms at $Ra = 10^8$, $RR = 2.6$ and $Pr = 0.7$: (a) $Re = 0$; (b) $Re = 10^3$; (c) $Re = 10^4$; and (d) $Re = 10^5$.

toward the mid-line ($\phi = 0°$) of the annulus. This demonstrates that the effect of the buoyant convection is larger than the centrifugally forced convection. For fixed Reynolds number, Table 1 shows that $\overline{Nu}$ values increase with increasing Ra due to the increase in convection heat transfer. In the rotating annuli, flow induced by centrifugal effects along the inner cylinder is promoted, especially, in the low Ra regime. This decrease in $\overline{Nu}$ is higher at lower Ra when centrifugally forced convection is predominant. For example, when Re increases from 0–10^5, the decreasing rate in mean Nusselt number $\overline{Nu}$ with 40.78% and with 27.45% at $Ra = 10^7$ and 10^8, respectively.

4.3. *Effect of radius ratio* (R_o/R_i)

Another parameter, the radius ratio of the annulus, can significantly affect mixed convection in the gap. In the following cases, the gap-width has been maintained constant and the radii of inner and outer cylinders have been changed to achieve different radius ratios. Figure 11 depicts the streamlines and isotherms for various radius ratio with fixed $Ra = 10^9$, $Re = 10^4$ and $Pr = 0.7$. When RR decreases, based on the same gap-width L, the increasing of heat transfer area near-wall region comes up accordingly. The intensities of the recirculation, turbulent energy and turbulent viscosity increase with the decrease in radius ratio. The

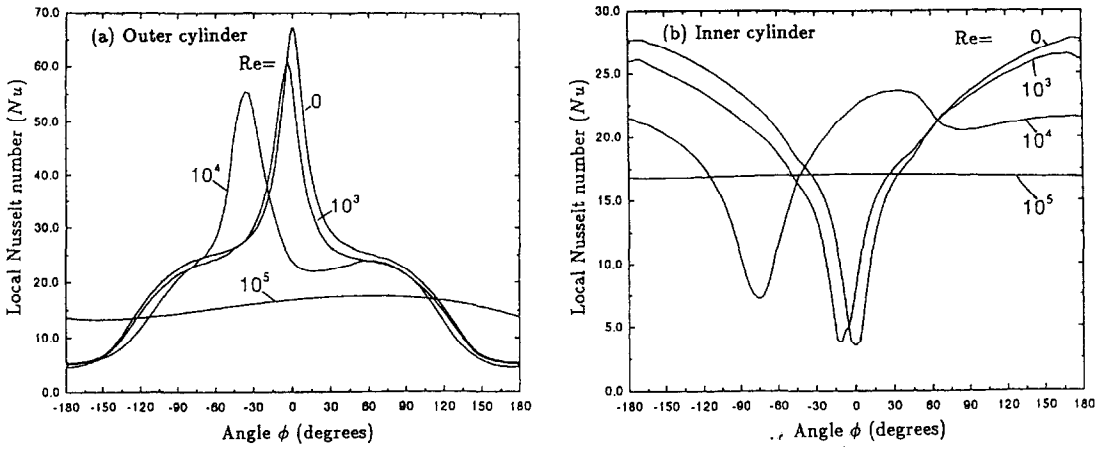

Fig. 8. Circumferential distribution of local Nusselt number Nu for various Reynolds number Re at $Ra = 10^8$, $RR = 2.6$ and $Pr = 0.7$: (a) outer cylinder; and (b) inner cylinder.

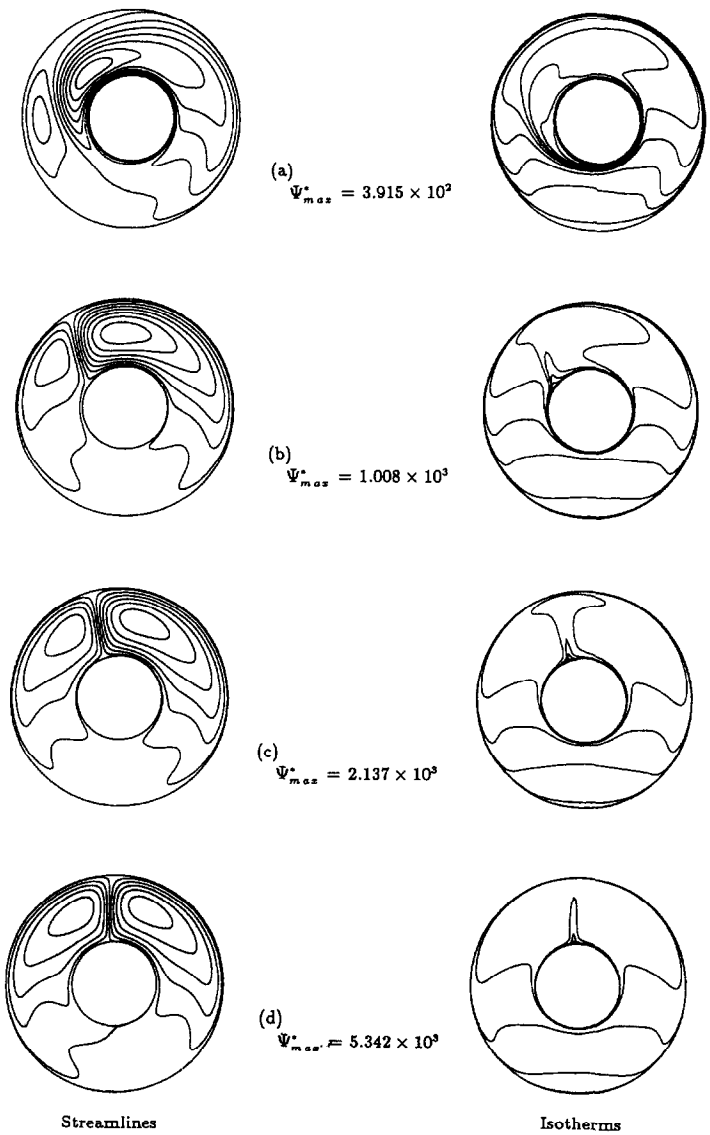

Fig. 9. Streamlines and isotherms at $Re = 10^4$, $RR = 2.6$ and $Pr = 0.7$: (a) $Ra = 10^7$; (b) $Ra = 10^8$; (c) $Ra = 10^9$; and (d) $Ra = 10^{10}$.

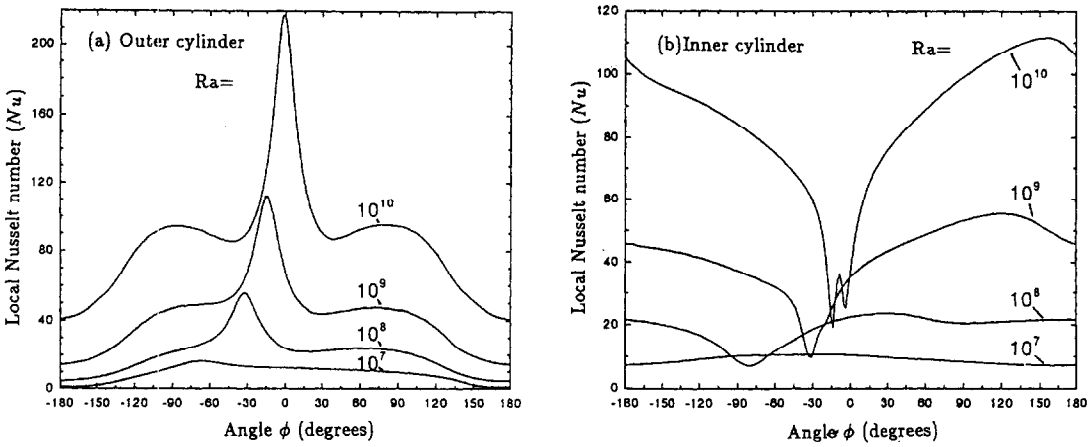

Fig. 10. Circumferential distribution of local Nusselt number Nu for various Rayleigh number Ra at $Re = 10^4$, $RR = 2.6$ and $Pr = 0.7$: (a) outer cylinder; and (b) inner cylinder.

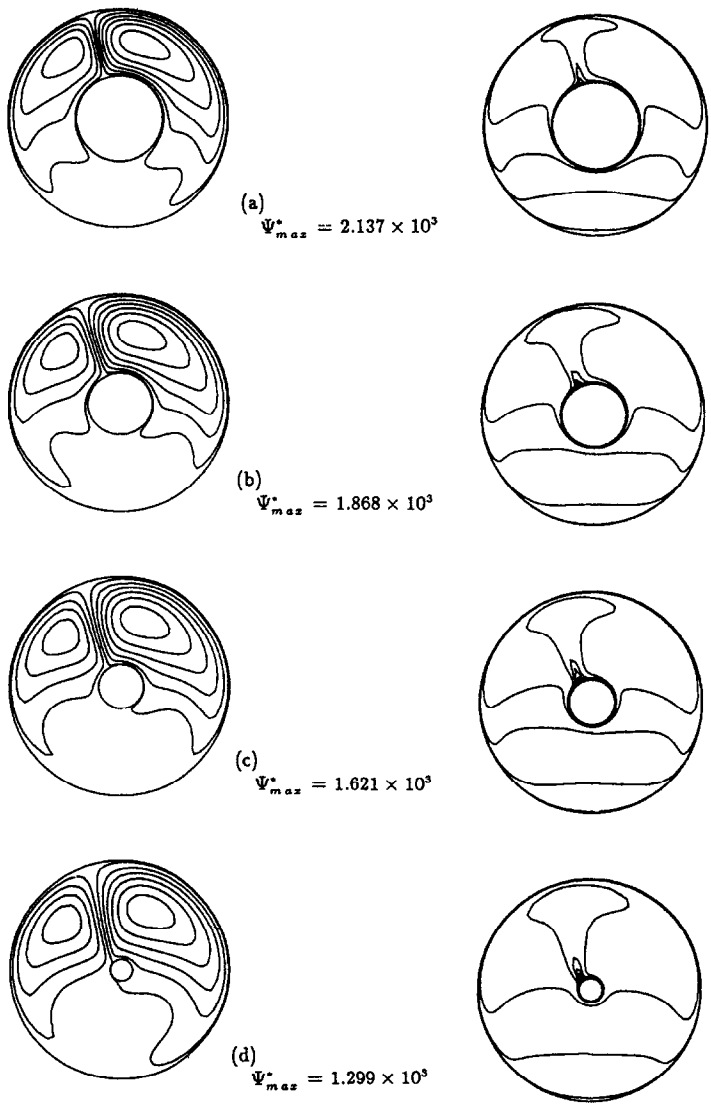

Fig. 11. Streamlines and isotherms at $Ra = 10^9$, $Re = 10^4$ and $Pr = 0.7$: (a) $RR = 2.6$; (b) $RR = 3.5$; (c) $RR = 5.0$; and (d) $RR = 10$.

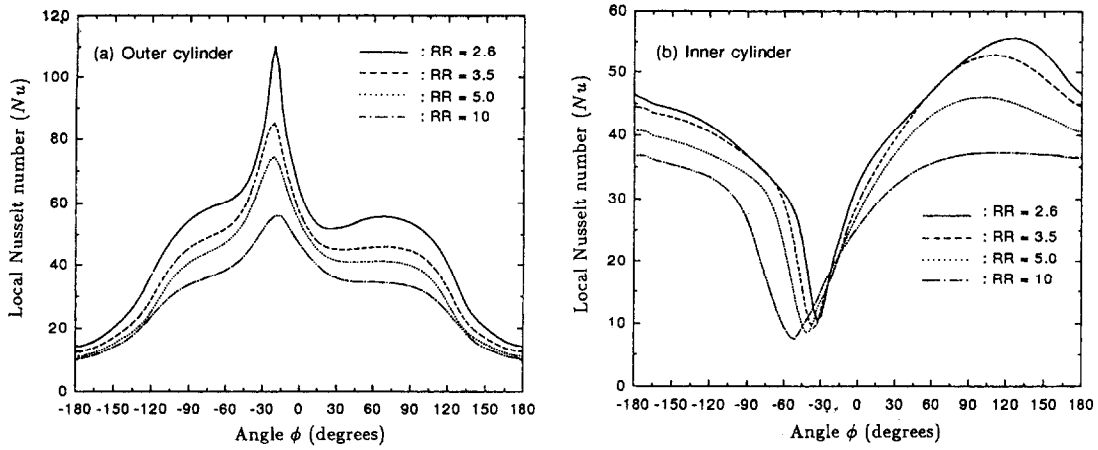

Fig. 12. Circumferential distribution of local Nusselt number Nu for various radius ratios RR at $Ra = 10^9$, $Re = 10^4$ and $Pr = 0.7$: (a) outer cylinder; and (b) inner cylinder.

local Nusselt number distribution is illustrated in Fig. 12. The variations of Nu become more uniform and monotonic when the radius ratio increases. When RR increases, the maximum local heat flux on the outer cylinder decreases and moves downward near the midline ($\phi = 0°$). On the other hand, the minimum local heat flux on the inner cylinder decreases and moves to the descending side in the annulus. At constant Ra and Re, Table 1 shows that $\overline{Nu}$ values decrease with increasing RR value due to greater centrifugal effects. This decrease in heat transfer over the rotating case value is higher at higher RR. For instance, when Re increases from 0–10^4, the decreasing rate in $\overline{Nu}$ with 16.99% for $RR = 10$ and $Ra = 10^9$ compared with 1.8% for $RR = 2.6$ and $Ra = 10^9$.

5. CONCLUDING REMARKS

Numerical simulation has been obtained for turbulent mixed-convection of air in an annulus consisting of two concentric horizontal cylinders, one being a cooled outer cylinder and the other a heated, rotating, inner cylinder. The following major conclusions can be drawn from this study.

1. In order to correct the deficiency, the over-prediction of turbulence energy around the impingement region by the Launder–Sharma model, it is essential to depress the turbulence energy in the impingement region. This has been achieved by adopting the Kato–Launder modification, which gives a much more satisfactory prediction than that of the Launder–Sharma model in the impingement region.
2. For all configurations, the results indicate that the mean Nusselt number, $\overline{Nu}$, increases with an increase in Ra, but decreases with an increase in the Reynolds number, Re, or radius ratio, RR.
3. The higher Reynolds number can enhance the strength of the secondary flow, as evidenced by the increasing values of the maximum streamfunction Ψ_{max}. The locations of the thermal plume and the maximum streamfunction Ψ_{max} are moved to the descending side, in accordance with the peak values of the local Nusselt number around the outer and inner cylinders. When $Re \geqslant 10^5$, the conduction effect becomes predominant in the gap.
4. In the centrifugal annulus with a stronger buoyancy-driven turbulence flow ($Ra > 10^9$), an interesting phenomena, the peak value of the Nusselt number distribution occurs in the vicinity of the thermal plume region, is firstly discovered and discussed. This peak phenomena is due to the occurrence of a reverse eddy flow at the plume region which gives rise to a reduction in the local heat transfer rate.
5. At lower Ra and higher Re, the centrifugal effects in the vicinity of the inner cylinder are promoted. An increase in the centrifugal effects results in a decrease in the mean Nusselt number. The decreasing rate in $\overline{Nu}$ is higher at lower Ra as well as higher RR because centrifugally forced convection is the dominant mode of heat transfer.

Acknowledgement—The authors are indebted to the referees for their valuable comments and, thus, the improvement of this paper.

REFERENCES

1. Yang, H. Q., Diffusion-controlled mass transfer from a rotating cylinder. *Numerical Heat Transfer A*, 1993, **23**, 303–318.
2. Yang, K. T., Yang, H. Q. and Lloyd, J. R., Rotational effects on natural convection in a horizontal cylinder. *AIChE Journal*, 1988, **34**, 1627–1633.
3. Prud'homme, M. and Robillard, L., Natural convection in an annular fluid layer rotating at weak angular velocity. In *Proceedings of the 4th International Symposium on Transport Phenomena, Heat and Mass Transfer*. Sydney, N.S.W., 1991, p. 38.

4. Kuehn, T. H. and Goldstein, R. J., An experimental study of natural convection heat transfer in concentric and eccentric horizontal cylindrical annuli. *ASME Journal of Heat Transfer*, 1978, **100,** 635–640.
5. Bishop, E. H., Heat transfer by natural convection of helium between horizontal isothermal concentric cylinders at cryogenic temperature. *ASME Journal of Heat Transfer*, 1988, **110,** 109–115.
6. Mcleod, A. E. and Bishop, E. H., Turbulent natural convection of gases in horizontal cylinders annului at cryogenic temperatures. *International Journal of Heat and Mass Transfer*, 1989, **32,** 1967–1978.
7. Desai, C. P. and Vafai, K., An investigation and comparative analysis two- and three-dimensional turbulent natural convection in a horizontal annulus. *International Journal of Heat and Mass Transfer*, 1994, **37,** 2475–2504.
8. Farouk, B. and Guceri, S. I., Laminar and turbulent natural convection in the annulus between horizontal concentric cylinders. *ASME Journal of Heat Transfer*, 1982, **104,** 631–639.
9. Launder, B. E. and Spalding, D. B., The numerical computation of turbulent flows. *Computer Methods of Applied Mechanics Engineering*, 1974, **3,** 269–289.
10. Henkes, R. A. W. M., Van Der Vlugt, F. F. and Hoogendoorn, C. J., Natural convection in a square cavity calculated with low-Reynolds-number turbulence models. *International Journal of Heat and Mass Transfer*, 1991, **34,** 377–388.
11. Launder, B. E. and Sharma, B. I., Application of the energy-dissipation model of turbulence to the calculation of the flow near a spinning disk. *Letters of Heat and Mass Transfer*, 1974, **1,** 131–138.
12. Yap, C. R., Turbulent heat and momentum transfer in recirculating and impinging flow. Ph.D. thesis, UMIST, Manchester, 1987.
13. Kato, M. and Launder, B. E., The modelling of turbulent flow around stationary and vibrating square cylinders. In *Proceedings of the 9th Symposium, Turbulent Shear Flows*. Kyoto, 1993, pp. 10–14.
14. Ince, N. Z. and Launder, B. E., On the computation of buoyancy-driven flows in rectangular enclosures. *International Journal of Heat and Fluid Flow*, 1989, **10,** 110–117.
15. Kenjereš, S. and Hanjalić, K., Prediction of turbulent thermal convection in concentric and eccentric horizontal annuli. *International Journal of Heat and Fluid Flow*, 1995, **16,** 429–439.
16. Lien, F. S. and Leschziner, M. A., A general non-orthogonal finite volume collocated algorithm for turbulent flow at all speeds incorporating second-moment turbulence-transport closure, Part 1: computational implementation. *Computational Methods Applied in Mechanical Engineering*, 1993, **114,** 123–148.
17. van Leer, B., Towards the ultimate conservation difference scheme v, a second-order sequel to Godunov's method. *Journal of Computational Physics*, 1979, **32,** 101–136.
18. Patankar, S. V., *Numerical Heat Transfer and Fluid Flow*. Hemisphere, Washington D.C., 1980.